



# CHORUS

This is the accepted manuscript made available via CHORUS. The article has been published as:

## Role of $\pi$ -d hybridization in a 300-K organic-magnetic interface: Metal-free phthalocyanine single molecules on a bcc Fe(001) whisker

T. K. Yamada, Y. Yamagishi, S. Nakashima, Y. Kitaoka, and K. Nakamura

Phys. Rev. B **94**, 195437 — Published 28 November 2016

DOI: [10.1103/PhysRevB.94.195437](https://doi.org/10.1103/PhysRevB.94.195437)

# Role of $\pi$ - $d$ hybridization in 300-K organic-magnetic interface: metal-free phthalocyanine single molecules on bcc Fe(001)-whisker

T. K. Yamada<sup>1,2\*</sup>, Y. Yamagishi<sup>1</sup>, S. Nakashima<sup>1</sup>, Y. Kitaoka<sup>3</sup>, and K. Nakamura<sup>4</sup>

1. Graduate School of Advanced Integration Science, Chiba University, 1-33 Yayoi-cho, Inage-ku, Chiba 263-8522, Japan

2. Molecular Chirality Research Center, Chiba University, 1-33 Yayoi-cho, Inage-ku, Chiba 263-8522, Japan

3. National Institute of Advanced Industrial Science and Technology (AIST), Spintronics Research Center, 1-1-1 Umezono, Tsukuba, Ibaraki, 305-8568, Japan

4. Department of Physics Engineering, Mie University, 1577, Kurimamachiya-cho, Tsu City, 514-8507, Mie, Japan

The realization of single molecular electronics is considered the next frontier to addressing and sustaining the storage needs of the future. In order to realize a single molecular device working at 300 K, two conditions must be satisfied: firstly, there must be no molecular diffusion, i.e., robust bonding between molecules and the contacting electrode, and secondly, stable electronic interface states. In this study, using a combination of 7-K and 300-K ultrahigh vacuum scanning tunneling microscopy/spectroscopy experiments and theoretical ab-initio calculations, we investigated the adsorption of  $\pi$ -conjugated metal-free phthalocyanine (Pc) single molecules onto an Fe(001) whisker single crystal along with the resulting electronic interface structures. The Pc/Fe(001) system was found to prevent molecular diffusion even at 300 K, due to strong adsorption as well as the presence of a larger diffusion barrier than that of the Pc/Ag(001) system, in which molecules are known to diffuse at 300 K. The origin of such a robust bonding was studied by recovering the sample local density of states (LDOS) with the normalized  $(dI/dV)/T$  curves, which LDOS peaks are successfully explained by theoretical calculations.

Keywords: organic molecule, scanning tunneling microscopy, ab initio calculations, molecular electronics, room-temperature functionality

## I. INTRODUCTION

The realization of single molecule devices is considered the next frontier to addressing and sustaining the storage needs of the future. In order to realize a single molecule junction working at 300 K, one condition must be satisfied: there must be robust bonding between molecules and the contacting electrode. The drastic increase in the use of computers and the internet has led to an increasing demand for high-capacity storage devices. Within current limitations in terms of resources and energy, nanotechnology and nanomaterials, which have aided in significantly reducing device sizes, have been

considered as a key solution to building devices that can address the memory needs of the future. In this backdrop, researchers have focused on nanomaterials such as carbon nanotubes, graphene, and molecular films to realize compact and flexible electronic devices [1-8]. Single molecules with sizes less than 1 nm have attracted attention as potential nanomaterials for future electronic devices [9-38].

Single organic molecules adsorbed onto various electrodes have been studied using both scanning tunneling microscopy (STM) as well as STM break-junction approaches. Insulating electrodes such as MgO, NaCl, and CuN [9-11] are powerful templates to visualize intrinsic molecular HOMO/LUMO states. Electronic interactions determine the bonding strength between  $\pi$ -conjugated single organic molecules and substrate electrodes, i.e., the insulating electrode exhibits negligible electronic interaction with the substrate.

Metallic substrates, mainly noble metals such as Au, Ag, Cu, and Pt, are also frequently used to realize phenomena such as Kondo resonance [12-23]. It is well-known that  $\pi$ -conjugated single molecules adsorbed onto noble metal electrodes such as fcc Au, Ag, Cu, or Pt, diffuse and form a two-dimensional ordered film at 300 K [20,22-25]. Because the molecules move across the noble metal electrode surface, in break-junction measurements, the single molecule can “fit” between the two electrodes [32-38]. Noble metal surfaces, in which mainly  $s$  or  $p$  states are dominant near the Fermi energy ( $E_F$ ), interact weakly with the molecule, essentially through the process of physisorption.

With metal-free single organic molecules supported by  $3d$  magnetic metals such as Fe, Co, Cr, and Mn, giant magnetoresistance (GMR) junctions have been successfully realized in a spin-polarized STM; the GMR value thus achieved was +60% for [Co(111)/H<sub>2</sub>Pc/Co(111)], -50% for [Mn(001)/H<sub>2</sub>Pc/Fe(110)], and -30% for [Fe/C<sub>60</sub>/Cr] single molecular junctions [14-16]. The interfaces between organic molecules and  $3d$  magnets appear to be spin-polarized even without the presence of magnetic ions in molecules due to hybridization between the  $d$  and  $\pi$  states, and thus, the molecules are likely chemisorbed; consequently, the distance between the substrate and the molecule is less than that in the physisorption case due to the strong nature of chemisorbed bonds.

In this study, metal-free phthalocyanine (H<sub>2</sub>Pc) single molecules are investigated as one of the ideal metal-free  $\pi$ -conjugated molecules by means of ultra-high vacuum (UHV) scanning tunneling microscopy and spectroscopy (STM/STS) at 7 K and

room temperature (RT). We focus on using a bcc-Fe(001)-whisker single crystal as the substrate electrode since the procedure to obtain a uniform surface, distinct electronic spin structures, and clear magnetic domain patterns for this single crystal has been well studied [39-41]. Further, whiskers prepared via the chemical vapor deposition method contain extremely low concentrations of impurities when compared with those in commercial Fe single crystals. 0.1 ML H<sub>2</sub>Pc molecules were adsorbed on the Fe(001)-whisker at 300 K. Different types of adsorption sites and new LDOS peaks were confirmed. Ab-initio calculations identified the origin of new interface state peaks, i.e., hybridization of molecular  $\pi$  and Fe(001)  $d$  states. Different LDOS inside single H<sub>2</sub>Pc molecules are confirmed experimentally and theoretically. With a comparison of H<sub>2</sub>Pc/Ag(001), where no hybridization of  $\pi$ - $d$  states, H<sub>2</sub>Pc molecules on Fe(001) were found to have more than three times higher diffusion barrier and adsorption energy. Experimentally H<sub>2</sub>Pc molecules on Fe(001) did not diffuse and immobilize by STM manipulation, indicating worse knowledge to realize 300 K single molecular devices.

## II. METHODS and EXPERIMENTALS

### A. STM and spectroscopy measurements

STM experiments were performed at 7 K and 300 K in ultrahigh vacuum (UHV, base pressure  $<8 \times 10^{-9}$  Pa). One of the most effective techniques for precisely measuring the LDOS of 1-nm-size molecules is tunneling spectroscopy with an STM setup, which is known as scanning tunneling spectroscopy (STS) [24]. STS measurements were performed by opening the feedback loop of the tunneling current, i.e., fixing the tip-sample separation ( $z$ ). The tunneling current was measured at each pixel by varying the sample voltage to obtain the  $I(V)$  curves, where zero voltage corresponds to the Fermi energy. The differential conductivity ( $dI/dV$ ) curves were obtained by numerical differentiation of the  $I(V)$  curves. The LDOS was obtained by the normalization of  $dI/dV$  curves using the  $T$  background, i.e.,  $(dI/dV)/T$  below the Fermi energy indicates occupied LDOS and  $(dI/dV)/T$  above the Fermi energy indicates unoccupied LDOS, where  $T$  denotes the fitted tunneling probability functions:  $T = a \exp(-2z\sqrt{\phi - eV/2}) + b \exp(-2z\sqrt{\phi + eV/2})$ , where  $a$  and  $b$  denote fitting parameters,  $\phi$ : averaged barrier height between tip and sample, and  $z$ : tip-sample separation [24,42-45]. In this study, we used  $\phi=4.5$  eV and  $z=10$  Angstroms, but we also tested the normalization with different  $\phi$  (4.0-5.5 eV) and  $z$  (5-11 Angstroms), while always we succeeded to recover the peaks at the same energy positions within  $\pm 20$  meV (see also ref.[24]).

### B. Sample and tip preparations

STM tungsten (W) tips were electrochemically etched from W wires ( $\phi = 0.3$  mm, purity 99.9%) in air using aqueous KOH.

The tip was rinsed with hot water and acetone and subsequently transferred into the load-lock chamber of our STM setup. The apex of the W tip was annealed to obtain an impurity-free apex under UHV conditions [46].

Fe-whisker single crystals were grown by using the chemical vapor deposition (CVD) technique to obtain high-purity Fe samples [39-41]. As shown in Fig.1(a), the FeCl<sub>2</sub> powder was set in the quartz tube inside the furnace. By flowing H<sub>2</sub> gas into the tube at 750 °C Fe-whiskers were grown inside the tube (see Fig.1(b)). Scanning electron microscopy (SEM) image in Fig.1(c) shows that one whisker has rectangular shape with a 10-50 mm length and a 0.1-1 mm side. X-ray Laue image in Fig.1(d) confirmed that the our Fe-whiskers have bcc (001) surfaces at the side planes. Magnetic imaging by SEM with polarization analysis (SEMPA) showed magnetic domains of the Fe-whisker. Typical size is 0.5×1.0 mm. Easy axis is <100> direction (long axis). The whisker that was introduced from air into the UHV chamber was first cleaned by Ar<sup>+</sup> sputtering and flattened by annealing up to 870 K for nearly two dozen times. Before STM measurements, the whisker was sputtered at 870 K for 30 min. The annealing was stopped 5 min after stopping the sputtering, which produced a clean and atomically flat Fe(001) surface. Figure 1(f) shows a topographic STM image of the Fe(001)-whisker single crystal at room temperature in ultrahigh vacuum (UHV). Atomic terraces larger than 100 nm are observed. The atomically resolved STM image in Fig. 1(g) indicates the presence of bcc (001) symmetry.

Commercial metal-free  $\pi$ -conjugated phthalocyanine (H<sub>2</sub>Pc) powder (Alfa Aesar, purity 95%) was purified by sublimation at 653 K and recrystallization at 473 K under a pressure of 10<sup>-3</sup> Pa (yield 30%). Nuclear magnetic resonance (NMR) and infrared spectra of the samples were used to confirm the absence of impurities after purification. The clean H<sub>2</sub>Pc powder was placed in a crucible, which was set in a molecular chamber and heated to 550 K. H<sub>2</sub>Pc molecules were deposited on the Fe(001) whisker in a UHV preparation chamber and subsequently transferred to an analytical STM chamber under UHV.

### C. Ab initio calculations

Calculations were carried out based on the generalized gradient approximation (GGA) [47] by using the full-potential linearized augmented plane-wave (FLAPW) method with single-slab geometry [48-50]. LAPW basis sets with cutoffs of  $|k + G| \leq 3.6$  a.u.<sup>-1</sup> and muffin-tin (MT) sphere radii of 2.2 a.u. for Ag and Fe, 1.2 a.u. for N and C, and 0.8 a.u. for H were used; lattice harmonics with angular momenta up to  $l = 8$  for Ag and Fe, 6 for N and C, and 4 for H were employed to expand the charge and spin densities. As a model, we adopted a single H<sub>2</sub>Pc molecule on a three-layer Ag(001) [and

Fe(001)] slab with four different adsorption sites, wherein the center of the molecule locates at the hollow, top (T), and saddle (B1 and B2) sites on the substrate surface. The in-plane bulk lattice constants of Ag and Fe were assumed, and the atomic positions of H<sub>2</sub>Pc and the substrate up to the second layer from the surface were fully optimized by atomic force calculations while the layer–layer distance on the opposite side was fixed to the corresponding bulk values.

### III. RESULTS AND DISCUSSIONS

We deposited about 0.1 ML H<sub>2</sub>Pc molecules on the Fe(001)-whisker substrate at 300 K in UHV and subsequently loaded the sample into the STM. STM/STS measurements were performed at 7 K and 300 K. H<sub>2</sub>Pc molecules were observed like four-leaf clover on the Fe(001) as shown in Fig. 2(a), i.e., H<sub>2</sub>Pc single molecules did not “stand”, but “lay” on the Fe(001) as hybridize the molecular  $\pi$  and Fe(001)  $d$  states. Each single molecule did not adsorb randomly. They follow to adsorb in particular directions. We confirmed three adsorption types: type A marked by black arrows, B marked by white arrows, and C marked by the circle. 56, 39, and 5 % of the adsorbed molecules on Fe(001) are type A, B, and C, respectively, suggesting that the type A molecules are the most energetically stable.

An enlarged image of the type A molecules is shown in Fig.2(b). Single H<sub>2</sub>Pc molecules were observed as an assemble of four bright protrusions. Its line profile (at  $V_s = -1V$ ) shows that the molecule has about 200 pm height on Fe(001) and the center is about 50 pm lower. The four bright protrusions are likely four side groups of the H<sub>2</sub>Pc. We call the center as “core” and the side groups as “arms”. The type A molecule adsorbed in parallel to [010].

The type B molecules could be the second most stable adsorption site. Its enlarged image is shown in Fig.2(c). Similar to the type A molecule, four bright protrusions were observed, about 200 pm height. The type B molecules adsorb about  $23 \pm 2$  degrees out of [010].

Rarely, we observed the type C molecule. The inset image in Fig. 2(a) shows an enlarged image. Different from type A and B molecules, type C molecule had extra protrusion at the core, i.e., something might exist at the center of the H<sub>2</sub>Pc molecule. The type C molecule tilted about  $45 \pm 2$  degrees from [010]. By a chance, there is possibility to enter at the core. Possible candidates are an Fe atom from the substrate, a W atom from the tip, and an impurity atoms such as C or O. Thus, the type C molecules might not be H<sub>2</sub>Pc.

We investigated local density of states (LDOS) of the type A, B, and C single molecules observed in Fig.2 by using STS. Figure 3 shows STS results obtained on the type A molecule. Figure 3(a) shows  $dI/dV$  curves obtained at the core (black

circles) and the Fe(001) substrate (grey circles) at 7 K. On the substrate, the sharp peak at +0.17 eV above the Fermi energy (i.e., the minority *d* states) proves that the observed surface is the bcc-Fe(001) substrate [39,41].

Compared to the Fe(001), the  $dI/dV$  curve at the core shows peaks around  $-0.3$  eV and  $+0.2$  eV, and also a shoulder around  $+0.8$  eV. These buried LDOS peaks are successfully recovered in normalized  $(dI/dV)/T$  curve by its fitted  $T$  function (dotted line). Figure 3(b) shows the obtained  $(dI/dV)/T$  curve (black circles). LDOS peaks were investigated by fitting with Gaussian functions. The fitting curve is shown as a black line. Obtained Gaussian peaks are named I, II, III, and IV, which energy positions are peak I:  $-0.22 \pm 0.16$  eV, peak II:  $+0.10 \pm 0.05$  eV, peak III:  $+0.21 \pm 0.11$  eV, and peak IV:  $+0.53 \pm 0.23$  eV (see Table 1).

Next, we performed STS measurements at 300 K, where LDOS peaks are expected to be broadened due to thermal fluctuation. Figure 3(c) shows a  $(dI/dV)/T$  curve (black circles) obtained at 300 K with a different tip (tip No.2). The black line shows an obtained fitting curve by using five Gaussian functions: peak I:  $-0.29 \pm 0.18$  eV, peak II:  $+0.14 \pm 0.08$  eV, peak III:  $+0.29 \pm 0.12$  eV, peak IV:  $+0.52 \pm 0.18$  eV, and peak V:  $-0.84 \pm 0.26$  eV. The peaks I-IV exist around the same energy positions as the peaks obtained at 7 K. On the other hand, the peak V around  $-0.85$  eV was only observed with the tip No.2, therefore we identify that the peak V is a tip state (see Table 1).

A topographic image and a  $dI/dV$  map at  $+0.9$  V of the type A molecule are shown in Fig. 3(d). In the  $dI/dV$  map, the arms appears darker and the core appears brighter, showing different LDOS exist inside the single molecule. A  $(dI/dV)/T$  curve obtained at the arms is shown in Fig. 3(d): peak I:  $-0.30 \pm 0.15$  eV, peak II:  $+0.18 \pm 0.09$  eV, peak III:  $+0.32 \pm 0.13$  eV, and peak IV:  $+0.56 \pm 0.25$  eV. The core and the arms have the LDOS peaks at the same energy positions, only the amplitude is different.

Thus, we experimentally confirmed that the free-standing HOMO/LUMO are significantly influenced by the contact of the molecule with Fe(001) via chemisorption.

In the same way,  $(dI/dV)/T$  curves obtained at the type B molecule are shown in Figs. 4(a) and (b). The  $dI/dV$  map of the type B molecule in (a) showed the arms appear darker and the core appear brighter, similar to the type A, indicating that the core has higher LDOS amplitude. Obtained peak energy positions are peak I:  $-0.31 \pm 0.16$  eV, peak II:  $+0.18 \pm 0.07$  eV, peak III:  $+0.31 \pm 0.14$  eV, and  $+0.58 \pm 0.37$  eV for the core, and peak I:  $-0.29 \pm 0.15$  eV, peak II:  $+0.19 \pm 0.10$  eV, peak III:  $+0.34 \pm 0.15$  eV, and peak IV:  $+0.58 \pm 0.27$  eV for the arms (see Table 1). Comparing with the type A, for the all peak energy positions are identical. It is clear there is no big difference in the LDOS between the type A and B molecules.

Finally, we performed spectroscopy measurements for the type C molecule. Results are shown in Figs. 4(c) and (d). The core likely includes an extra atom. Obtained peak positions are peak I:  $-0.31 \pm 0.16$  eV, peak II:  $+0.25 \pm 0.12$  eV, peak III:  $+0.45 \pm 0.08$  eV, and peak IV:  $+0.64 \pm 0.24$  eV for the core, and peak I:  $-0.28 \pm 0.14$  eV, peak II:  $+0.23 \pm 0.12$  eV, peak III:  $+0.45 \pm 0.19$  eV, and peak IV:  $+0.79 \pm 0.30$  eV for the arms (see Table 1). The peak I did not change so much from the type A and B, while the peak II, III, and IV positions shifted clearly. For example, the peak III shifted to  $+0.45$  eV from around  $+0.3$  eV for the type A and B. The  $(dI/dV)/T$  curve suggested that the type C could not be H<sub>2</sub>Pc.

First principle calculations were performed to investigate the experimentally found four peaks (I, II, III and IV) in  $(dI/dV)/T$  curves in Fig. 3. Figure 5 shows calculation results of the energetically stable type A molecule. Figure 5(a,b) shows calculated LDOS of a free-standing H<sub>2</sub>Pc molecule at the core (a) and the arms (b). HOMO-LUMO states are observed with a gap of about 1.5 eV. Upper and lower panels show majority and minority spin states, respectively. The free-standing H<sub>2</sub>Pc is not spin-polarized.

Majority and minority spin states of the H<sub>2</sub>Pc on Fe(001) were calculated as shown in Fig. 5(c,d) with the energetically stable configuration in Fig. 5(e) based on experimentally observed configuration in Fig.2. Adsorption energy at the four-fold hollow site was energetically the most stable (Fig. 6(c)). In Fig. 5(e), yellow, grey, and blue spheres denote nitrogen, carbon, and hydrogen atoms, respectively. The atoms marked by the red circles belong to the core, and the atoms marked by the blue circles belong to the arms. Figures 5(c) and (d) show LDOS at the core and the arms, respectively.

Between majority and minority spin states, significant difference is observed from  $-2$  eV to  $+2$  eV, i.e., spin-polarized, while this is not so surprising. Although, so far no report of H<sub>2</sub>Pc on Fe(001), phthalocyanine or porphyrin molecules on Mn(001), Fe(110), and Co(0001) have been reported to be spin-polarized when they contact with 3d magnetic substrates (so far all reported experiments were performed at low temperatures).

In Fig.3, we experimentally found four peaks around the Fermi energy. In the calculated LDOS in Fig. 5(c,d), we observed three peaks around the Fermi energy.

Comparing with Figs. 3 and 5(c,d) shows that the origin of the peaks II and III is the majority spin states (yellow area), and the peak I and IV peaks are mainly consist of the minority spin states. Similar to the core, at the arms, majority spin peak is observed at the peaks II and III, and minority spin peaks are observed at the peaks I and IV, while the peak amplitude is relatively smaller than the core.

Figures 5(f) and (g) show how the non-spin-polarized states of free-standing H<sub>2</sub>Pc in Figs. 5(a) and (b) change to spin-polarized states when H<sub>2</sub>Pc contacts with Fe(001). The longitudinal axis and horizontal axis denote energy and position, respectively. The molecular minority spin states hybridize with the Fe(001) minority spin states.

Figure 5(f) shows the minority spin states. The left hand side shows Fe(001) states. As shown in Fig. 3(a), Fe(001) has a strong minority  $d_{xz+yz}$  peak above the Fermi energy (the red line in Fig. 5(f)). The right hand side in Fig. 5(f), HOMO/LUMO states of the free-standing H<sub>2</sub>Pc are shown as black lines. When the H<sub>2</sub>Pc approaches to the Fe(001), the Fe(001) minority spin state and H<sub>2</sub>Pc LUMO minority spin state are energetically close, and the chemisorption of the H<sub>2</sub>Pc arises from the strong hybridization between the LUMO state and the localized state at the Fe surface, which pushes up the bonding and antibonding states in energy where electrons between the H<sub>2</sub>Pc and the Fe surface accumulate and deplete, respectively, as illustrated in the I and II in Fig. 5(h). On the other hand, as shown in Fig. 5(g), the Fe(001) does not have the majority spin peak around the Fermi energy. Therefore, the molecular LUMO majority spin state is less affected. As a result, LUMO majority spin state remains above the Fermi energy.

By following this simple hybridization mechanism, it is speculated that the experimentally observed peaks I and IV are the hybridized minority spin states, and the peaks II and III are the remained LUMO majority spin state. Indeed, since the peaks II and III, taken on molecules (at 0.14-0.18 eV), locate rather close to the surface states of the Fe(001) substrate (at around 0.17eV), the spectroscopic features of the substrate may be retained to some extent on the molecule. However, the cross section views of the density distribution of the calculated interface LDOS, as mentioned in Fig. 5(h), may rule out the substrate contribution since at the I and IV, the molecular  $\pi$  and the Fe(001)  $d$  states are hybridized while at the II and III, there is no hybridization. Thus, the substrate peaks have no measurable contribution to the molecule peaks and such unique hybridization is further supported at the Co(0001) surface experimentally when they contact with  $\pi$ -conjugated phthalocyanine molecules [51].

As already shown in Fig.2, metal-free H<sub>2</sub>Pc molecules were observed as “single” molecules on Fe(001) at 300 K. Spectroscopy measurements were able to be performed stably at 300 K, while such metal-free molecules are known to be diffused on noble metal substrates at 300 K and be formed films [20,24]. Here, we remark that electronic interactions determine the bonding strength between  $\pi$ -conjugated single organic molecules and substrate electrodes, i.e., the insulating electrode exhibits negligible electronic interaction with the substrate. Noble metal surfaces, in which mainly  $s$  or  $p$  states are

dominant near the Fermi energy ( $E_F$ ), interact weakly with the molecule, essentially through the process of physisorption.

Figure 6(a) shows LDOS of H<sub>2</sub>Pc molecules adsorbed on Ag(001), which is similar to the free-standing H<sub>2</sub>Pc in Fig. 5(a,b), i.e., the HOMO and LUMO states of the H<sub>2</sub>Pc molecule, even after the molecule is adsorbed onto the Ag(001) surface, do not change significantly from those of the free-standing molecule. This leads to weak physisorption, and therefore, single H<sub>2</sub>Pc molecules easily overcome the diffusion barrier by thermal assistance even at temperatures less than room temperature.

The interfaces between organic molecules and 3d magnets appear to be spin-polarized even without the presence of magnetic ions in molecules due to hybridization between the  $d$  and  $\pi$  states, and thus, the molecules are likely chemisorbed; consequently, the distance between the substrate and the molecule is less than that in the physisorption case due to the strong nature of chemisorbed bonds. Such chemisorption may prevent the diffusion of single molecules and generate strong bonding between single molecules and the electrode at 300 K.

Concretely, adsorption energy when the H<sub>2</sub>Pc molecule approaches to the Ag(001) and the Fe(001) was calculated. Here, Ag(001) was used as the reference for the diffusion case.

The total energy as a function of the molecule–substrate separation ( $d$ ) for adsorption at the H site was calculated (Fig. 6(b)) under the absence of relaxation for purposes of simplicity. The calculations clearly demonstrate that the adsorption energy on the Fe(001) surface ( $-4.2$  eV at  $\sim 0.15$  nm) is larger than that of the Ag(001) surface ( $-1.5$  eV at  $\sim 0.2$  nm) by a factor of about three. (The adsorption energy difference was assumed to be zero far from the surface at 430 pm.) It is noteworthy that the distances at the energy minimum are approximately equal to the apparent height of the molecules in the STM images, which values are about 0.15 nm and 0.20 nm on the Fe(001) and Ag(001) surfaces, respectively. These theoretical calculations indicate that a single H<sub>2</sub>Pc molecule does not diffuse on Fe(001) at 300 K, while H<sub>2</sub>Pc on Ag(001) is known to diffuse at 300 K.

To further confirm the robust adsorption of the H<sub>2</sub>Pc molecule onto the Fe(001) surface, the total energies at different adsorption sites of the H<sub>2</sub>Pc molecule,  $E_H$ ,  $E_T$ ,  $E_{B1}$ , and  $E_{B2}$ , on the Ag(001) and Fe(001) surfaces were calculated, assuming that the center of the molecule locates on the hollow site (H), top site (T), bridge site 1 (B1), and bridge site 2 (B2). In both surfaces, adsorption at the H site is found to be energetically the most favorable. Importantly, the energy differences of the T, B1, and B2 sites with respect to that of the H site,  $E_{\text{Site}} = E_{\text{Site}} - E_H$ , indicate that the H<sub>2</sub>Pc/Fe(001) system presents a

larger energy barrier to thermal diffusion when compared with that of the H<sub>2</sub>Pc/Ag(001) system. For the Ag(001) surface, the energy difference is about 0.1 to 0.2 eV/molecule along the [110], [100], and [010] directions, but for Fe(001), the corresponding values are 0.6, 0.9, and 1.0 eV, which values could thus be sufficiently large to prevent the diffusion of the H<sub>2</sub>Pc molecules even at room temperature. By using the Arrhenius equation with the calculated energy barriers, the average time that the molecules spends before diffusing to neighboring sites, e.g., the T sites, is confirmed to be significantly larger on the Fe substrate than that on the Ag substrate by factor of 10<sup>8</sup> even in a room temperature where the frequency factor is assumed to be same between the Fe and Au substrates.

The thermal stability of H<sub>2</sub>Pc molecules on Fe(001) was experimentally confirmed by means of consecutively obtained STM images of the same area. Figure 6(d) shows these images, which were sequentially acquired every 5 minutes. It is obvious that single molecules do not diffuse on Fe(001) at 300 K, which validates the theoretical prediction indicated in Fig. 6(b,c). The diffusion barrier on Fe(001) needs to be four times that on Ag(001) to prevent diffusion. We attempted to manipulate the single molecules by pushing them along the [110] direction using the STM tip because this direction has a lower barrier when compared with those of the [100] and [010] directions (Fig. 6(c)). The results of our “pushing” are shown in Fig. 6(e); in these cases, we attempted to move five single molecules at different tunneling resistances of  $1 \times 10^9 \Omega$  ( $V_s = -600$  mV,  $I = 600$  pA),  $2 \times 10^8 \Omega$  ( $V_s = -600$  mV,  $I = 3$  nA),  $2 \times 10^7 \Omega$  ( $V_s = -600$  mV,  $I = 30$  nA), and  $3 \times 10^6 \Omega$  ( $V_s = -100$  mV,  $I = 30$  nA); the molecules did not move in any of the five cases.

Such a robust bonding that cannot be broken by STM tip manipulation indicates the possibility of fabricating room-temperature single molecule junctions.

#### IV. CONCLUSIONS

Adsorption and electronic states of metal-free  $\pi$ -conjugated phthalocyanine single molecules adsorbed on the Fe(001)-whisker single crystal were studied by means of UHV-STM and STS at 7 K and 300 K. The single H<sub>2</sub>Pc molecules adsorbed with three orientations; type A is the most energetically stable, parallel to [100], type B is the second stable with a rotation of about 23 degrees from [100]. Rarely, type C molecules are observed with a rotation of about 45 degrees from [100]. The type C includes an extra atom at the core, possibly an Fe atom or an impurity atom. Type A and B have similar LDOS peaks. Our ab-initio calculations nicely recovers the experimentally obtained LDOS peaks, suggesting the hybridization process between the molecular LUMO and the Fe(001)  $d_{xz+yz}$  states. Since Fe(001) has a minority spin states

above the Fermi energy, hybridization mainly occur with the LUMO minority spin states, producing new bonding/antibonding states below/above the Fermi energy. On the other hand, LUMO majority spin states remains without hybridization by the  $d$  states, thus spin-polarized LDOS peaks are tailored around the Fermi energy. Further, even inside the same single molecule, core and arms (side groups) have different LDOS and spin-polarization, suggesting careful manners to deduce spin-polarization of the single molecules using STS. Studies of the H<sub>2</sub>Pc single molecules on Fe(001) firstly theoretically and experimentally verify that systematically we can diffuse or immobilize the  $\pi$ -conjugated single molecules at 300 K by selecting the contacting substrate, which is one of key knowledge for realization of 300-K single molecular devices. The H<sub>2</sub>Pc/Fe(001) system could be the first evidence to prove that the strong  $\pi$ - $d$  bonding can stop the molecule diffusion at room temperature.

## ACKNOWLEDGEMENTS

We thank Dr. D. T. Pierce (NIST) for his guidance regarding the chemical vapor deposition of the Fe whisker. We thank Prof. Dr. H. Ishii (Chiba Univ.) and Prof. Dr. Y. Noguchi (Meiji Univ.) for supporting purification of the molecules, Prof. Dr. F. Shibahara (Gifu Univ.) for NMR and IR measurements, and Mr. R. Nemoto for the Gaussian fittings. Computations were performed at Supercomputer Center, Institute for Solid State Physics, University of Tokyo, Center for Computational Materials Science, Institute for Materials Research, Tohoku University, and Research Institute for Information Technology, Kyushu University. This work was supported by JSPS KAKENHI Grant Number 23681018, 25110011, the Japan Science and Technology Agency (JST)-Improvement of Research Environment for Young Researchers, Chiba University Young Research-Oriented Faculty Member Development Program in Bioscience Areas, Casio Science Promotion Foundation, Asahi Glass Foundation, Hatakeyama Culture Foundation, The Association for the Progress of New Chemistry, Iketani Science and Technology Foundation, The Noguchi Institute, Ozawa Yoshikawa Memorial Electronics Foundation, Research Foundation for the Electrotechnology of Chubu, The Nakajima Foundation, The Futaba Electronics Memorial Foundation, and Shimadzu Foundation.

## References

- [1] A. C. Ferrari and D. M. Basko, *Nat. Nanotech.* **8**, 235 (2013).
- [2] S. Z. Butler, *et al.* *ACS Nano*, **7**, 2898 (2013).
- [3] S. Park, M. Vosguerichian, Z. A. Bao, *NANOSCALE* **5**, 1727 (2013).

- [4] Q. Zhang, J. Q. Huang, W. Z. Qian, Y. Y. Zhang, and F. Wei, *SMALL* **9**, 1237 (2013).
- [5] U. N. Maiti, W. J. Lee, J. M. Lee, Y. Oh, J. Y. Kim, J. E. Kim, J. Shim, T. H. Han, and S. O. Kim, *Adv. Mater.* **26**, 40 (2014).
- [6] Y. Zang, C. Z. Li, C. C. Chueh, S. T. Williams, W. Jiang, Z. H. Wang, J. S. Yu, and A. K. Y. Jen, *Adv. Mater.* **26**, 5708 (2014).
- [7] Y. H. Zhou, J. Zeng, L. M. Tang, K. Q. Chen, and W. P. Hu, *Organic Electronics* **14**, 2940 (2013).
- [8] B. O. Jahn, H. Ottosson, M. Galperin, and J. Fransson, *ACS Nano* **7**, 1064 (2013).
- [9] L. Gross, F. Mohn, N. Moll, P. Liljeroth, G. Meyer, *Science* **325**, 1110 (2009).
- [10] H. J. Shin, J. Jung, K. Motobayashi, S. Yanagisawa, Y. Morikawa, Y. Kim, M. Kawai, *Nat. Mater.* **9**, 442 (2010).
- [11] T. Miyamachi, M. Gruber, V. Davesne, M. Bowen, S. Boukari, F. Scheurer, G. Rogez, T. K. Yamada, P. Phresser, E. Beaurepaire, W. Wulfhekel, *Nat. Commun.* **3**, 938 (2012).
- [12] G. Schull, T. Frederiksen, M. Brandbyge, and R. Berndt, *Phys. Rev. Lett.* **103**, 206803 (2009).
- [13] J. Brede, N. Atodiresei, S. Kuck, P. Lazic, V. Caciuc, Y. Morikawa, G. Hoffmann, S. Bluegel, and R. Wiesendanger, *Phys. Rev. Lett.* **105**, 047204 (2010).
- [14] S. Schmaus, A. Bagrets, Y. Nahas, T. K. Yamada, A. Bork, F. Evers, and W. Wulfhekel, *Nat. Nanotechnol.* **6**, 185 (2011).
- [15] S. L. Kawahara, J. Lagoute, V. Repain, C. Chacon, Y. Girard, S. Rousset, A. Smogunov, C. Barreteau, *Nano Lett.* **12**, 4558 (2012).
- [16] A. Bagrets, S. Schmaus, A. Jaafar, D. Kramczynski, T. K. Yamada, M. Alouani, W. Wulfhekel, and F. Evers, *Nano Lett.* **12**, 5131 (2012).
- [17] M. Mannini, F. Pineider, P. Sainctavit, C. Danieli, E. Otero, C. Sciancalepore, A. M. Talarico, M. -A. Arrio, A. Cornia, D. Gatteschi, and R. Sessoli, *Nat. Mater.* **8**, 194 (2009).
- [18] M. Mannini, F. Pineider, P. Sainctavit, L. Joly, A. Fraile-Rodriguez, M. -A. Arrio, C. C. Moulin, W. Wernsdorfer, A. Cornia, D. Gatteschi, and R. Sessoli, *Adv. Mater.* **21**, 167 (2009).
- [19] L. Bogani, and W. Wernsdorfer, *Nat. Mater.* **7**, 179 (2008).
- [20] N. Tsukahara, K. Noto, M. Ohara, S. Shiraki, N. Takagi, Y. Takata, J. Miyawaki, M. Taguchi, A. Chainani, S. Shin, and M. Kawai, *Phys. Rev. Lett.* **102**, 167203 (2009).
- [21] T. Komeda, H. Isshiki, J. Liu, Y. F. Zhang, N. Lorente, K. Katoh, B. K. Breedlove, and M. Yamashita, *Nat. Commun.*

2 217 (2010).

[22] I. Chizhov, G. Scoles, and A. Kahn, *Langmuir* **16**, 4358 (2000).

[23] A. Scarfato, S. H. Chang, S. Kuck, J. Brede, G. Hoffmann, and R. Wiesendauer, *Surf. Sci.* **602**, 677 (2008).

[24] Y. Yamagishi, S. Nakashima, K. Oiso, and T. K. Yamada, *Nanotechnology* **24**, 395704 (2013).

[25] A. Zhao, Q. Li, L. Chen, H. Xiang, W. Wang, S. Pan, B. Wang, X. Xiao, J. Yang, J. G. Hou, and Q. Zhu, *Science* **309**, 1542 (2005).

[26] T. A. Jung, R. R. Schlittler, J. K. Gimzewski, H. Tang, and C. Joachim, *Science* **271**, 181 (1996).

[27] S. J. H. Griessl, M. Lackinger, F. Jamitzky, T. Markert, M. Hietschold, and W. M. Heckl, *J. Phys. Chem* **108**, 11556 (2004).

[28] P. A. Sloan, and R. E. Palmer, *Nature* **434**, 367 (2005).

[29] H. Yang, A. J. Mayne, G. Comtet, G. Dujardin, Y. Kuk, S. Nagarajan, and A. Gourdon, *Phys. Rev. B* **90**, 125427 (2014).

[30] C. Waeckerlin, *et al.* *Angew. Chem. Int. Ed.* **52**, 4568 (2013).

[31] H. C. Herper., *et al.* *Phys. Rev. B* **87**, 174425 (2013).

[32] T. Konishi, *et al.*, *J. Am. Chem. Soc* **135**, 1009 (2013).

[33] D. Xiang, H. Jeong, D. Kim, T. Lee, Y. Cheng, Q. Wang, and D. Mayer, *Nano Letters* **13**, 2809 (2013).

[34] M. L. Perrin, *et al.*, *Nat. Nanotech.* **9**, 830 (2014).

[35] Z. Li and E. Borguet, *J. Am. Chem. Soc* **134**, 63 (2012).

[36] M. Kiguchi, S. Nakashima, T. Tada, S. Watanabe, S. Tsuda, Y. Tsuji, and J. Terao, *SMALL* **8**, 726 (2012).

[37] K. Kaasbjerg, and K. Flensberg, *Phys. Rev. B* **84**, 115457 (2011).

[38] V. A. Sydoruk, *et al.*, *J. Appl. Phys.* **112**, 014908 (2012).

[39] J. A. Stroschio, D. T. Pierce, A. Davies, and R. J. Celotta, *Phys. Rev. Lett.* **75**, 2960 (1995).

[40] J. Unguris, R. J. Celotta, and D. T. Pierce, *Phys. Rev. Lett.* **79**, 2734 (1997).

[41] M. M. J. Bischoff, T. K. Yamada, C. M. Fang, R. A. de Groot, and H. van Kempen, *Phys. Rev. B* **68**, 045422 (2003).

[42] V. A. Ukraintsev, *Phys. Rev. B* **53**, 11176 (1996).

[43] T. K. Yamada, M. M. J. Bischoff, T. Mizoguchi, and H. van Kempen, *Surf. Sci.* **516**, 179 (2002).

[44] T. K. Yamada, M. M. J. Bischoff, G. M. M. Heijnen, T. Mizoguchi, and H. van Kempen, *Phys. Rev. Lett.* **90**, 056803 (2003).

- [45] L. Gerhard, T. K. Yamada, T. Balashov, A. F. Takacs, R. J. H. Wesselink, M. Daene, M. Fechner, S. Ostanin, A. Ernst, I. Mertig, and W. Wulfhekel, *Nat. Nanotech.* **5**, 792 (2010).
- [46] T. K. Yamada, T. Abe, N. M. K. Nazriq, and T. Irisawa, *Review of Scientific Instruments* **87**, 033703 (2016).
- [47] J. P. Perdew, K. Burke, and M. Ernzerhof, *Phys. Rev. Lett.* **77**, 3865 (1996).
- [48] E. Wimmer, H. Krakauer, M. Weinert, and J. A. Freeman, *Phys. Rev. B* **24**, 864 (1981).
- [49] M. Weinert, E. Wimmer, and A. J. Freeman, *Phys. Rev. B* **26**, 4571 (1982).
- [50] K. Nakamura, T. Ito, A. J. Freeman, L. Zhong, and J. Fernandez-de-Castro, *Phys. Rev. B* **67**, 014420 (2003).
- [51] C. Iacovita, M. V. Rastei, B. W. Heinrich, T. Brumme, J. Kortus, L. Limot, and J. P. Bucher *Phys. Rev. Lett.* **101**, 116602.

Figure captions.

Figure 1

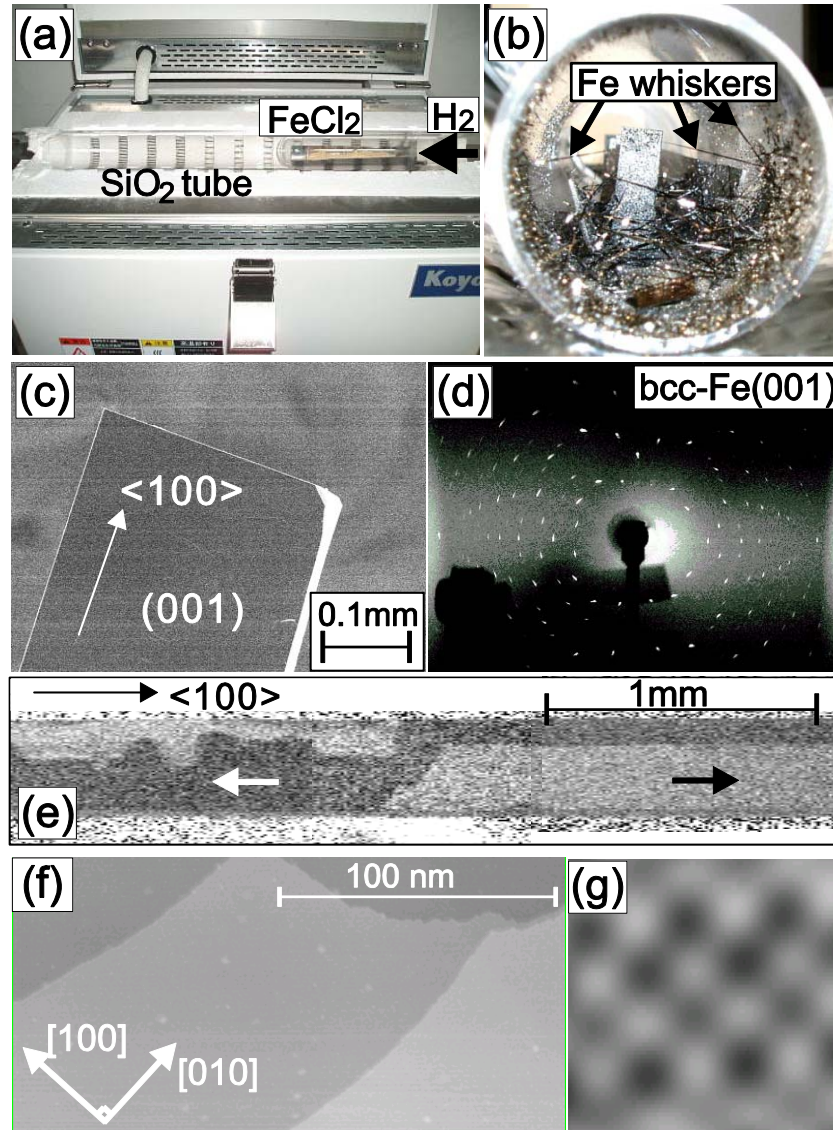


Fig.1: (a) A picture of a furnace growing Fe-whiskers from FeCl<sub>2</sub> powders with H<sub>2</sub> gas: chemical vapor deposition (CVD) process. (b) A picture of grown Fe-whiskers inside the SiO<sub>2</sub> tube. (c) Scanning electron microscopy (SEM) image of the single Fe-whisker. (d) X-ray Laue image obtained from the whisker. (e) Magnetic domain image by our home-built SEM with polarization analysis (SEMPA). (f) Scanning tunneling microscopy (STM) topographic images of the Fe(001) whisker surface (215 × 108 nm). (g) An atomically resolved STM image of Fe(001) (1.1 × 1.1 nm).

Figure 2

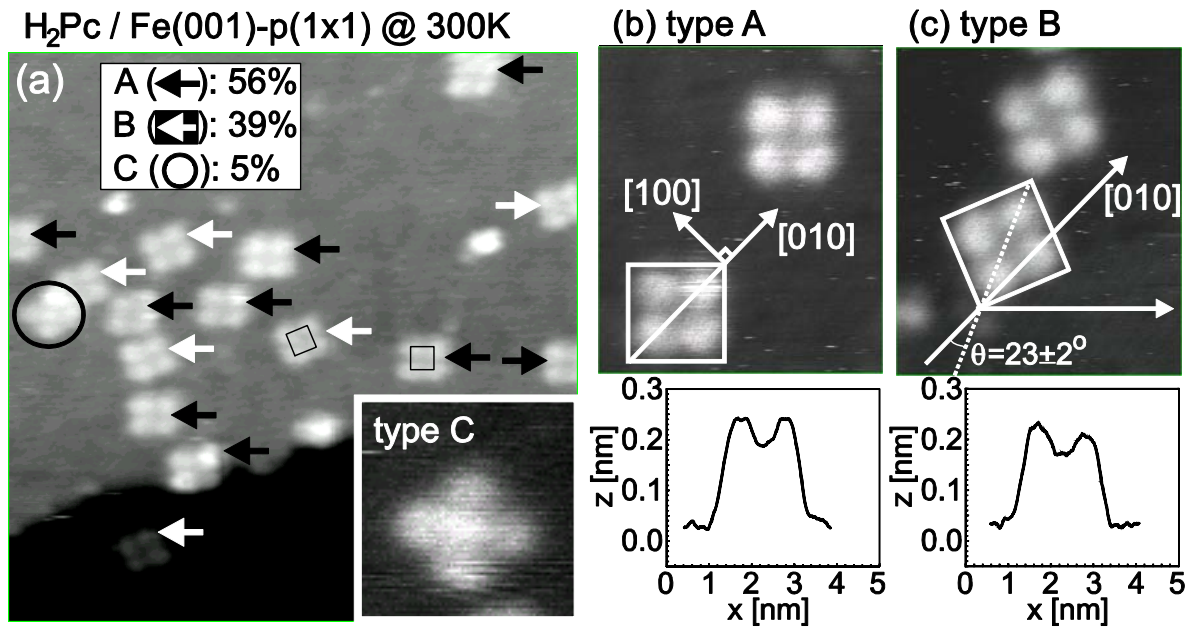


Fig.2: (a) STM topographic image of the Fe(001) substrate covered by 0.1 ML of  $\text{H}_2\text{Pc}$  molecules ( $V_S = -1.0$  V,  $I = 50$  pA,  $20 \times 20$  nm), observed at room temperature. The single molecules are observed. White and black arrows indicate type A and B molecules adsorbing on the bcc-Fe(001) with different orientations. Rarely, the molecule marked by the circle was observed: type C. The enlarged image (the inset in (a)) shows a protrusion at the core of the molecule, while no protrusion at the core for type A and B molecules. Adsorption probabilities are 56, 39, and 5 %, for type A, B, and C, respectively. (b) and (c) show enlarged STM topographic images and those line profiles of type A and B molecules ( $V_S = -1.5$  V,  $I = 300$  pA,  $5 \times 5$  nm).

Figure 3

Type A

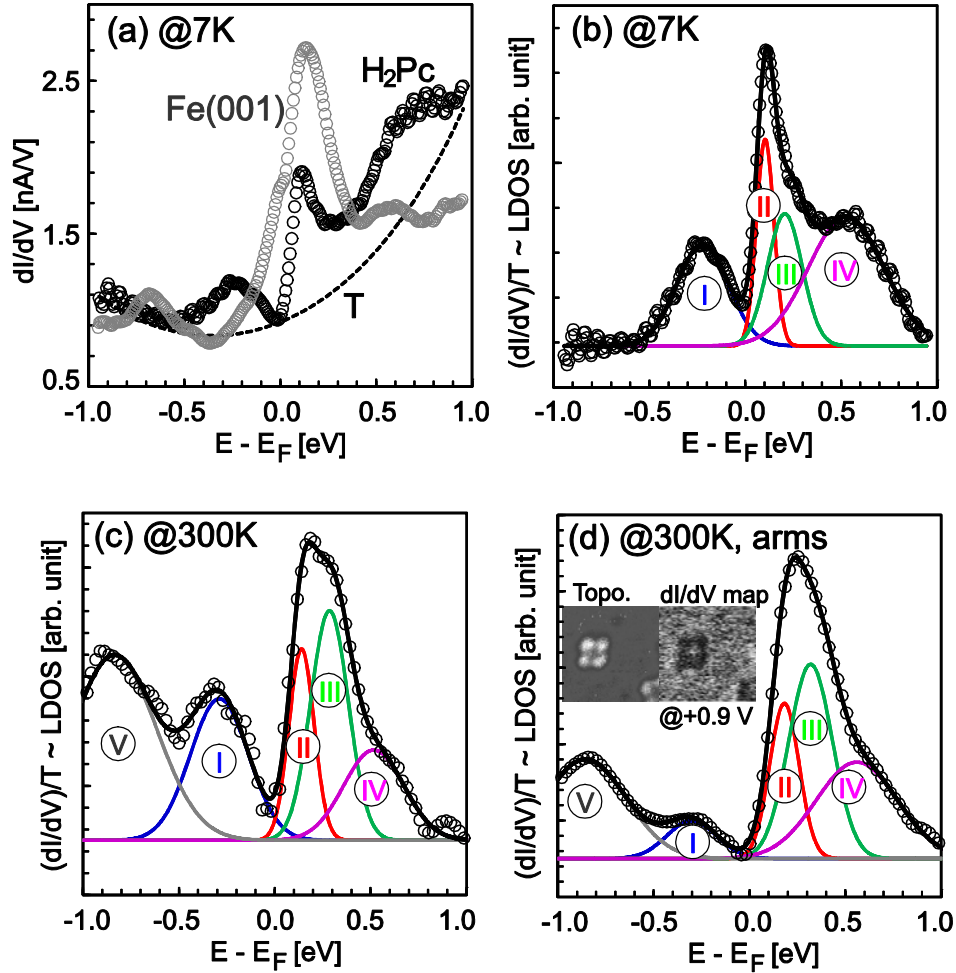


Fig.3: (color online) STS measurements at 7 K and 300 K performed on the single H<sub>2</sub>Pc molecules (type A) adsorbed on the Fe(001)-whisker.

(a)  $dI/dV$  curves ( $V_s = -0.5$  V,  $I = 500$  pA) were obtained at 7 K in UHV with the tip No.1 on the H<sub>2</sub>Pc single molecule (black circles) and the Fe(001) substrate (grey circles). A dotted line denotes a fitted  $T$  function. (b)  $(dI/dV)/T$  curve (black circles) obtained from the  $dI/dV$  curve in (a) with the fitted  $T$ . The  $(dI/dV)/T$  curve was fitted with Gaussian curves. The fitted curve is shown as a black line. Obtained Gaussian peaks were used to determine LDOS peak energy positions labeled I (blue), II (red), III (green), and IV (pink).

(c,d)  $(dI/dV)/T$  curve (black circles) obtained on the single H<sub>2</sub>Pc molecule at 300 K with a different tip (tip No.2). The  $(dI/dV)/T$  curves were fitted with Gaussian curves. The fitted curves are shown as black lines. Obtained Gaussian peaks were used to determine LDOS peak energy positions labeled I (blue), II (red), III (green), IV (pink), and V (grey). (c) was obtained at the core and (d) was obtained at the arms. Insets in (d) ( $5 \times 5$  nm) show a topographic image and a  $dI/dV$  map at +0.9 V.

Figure 4

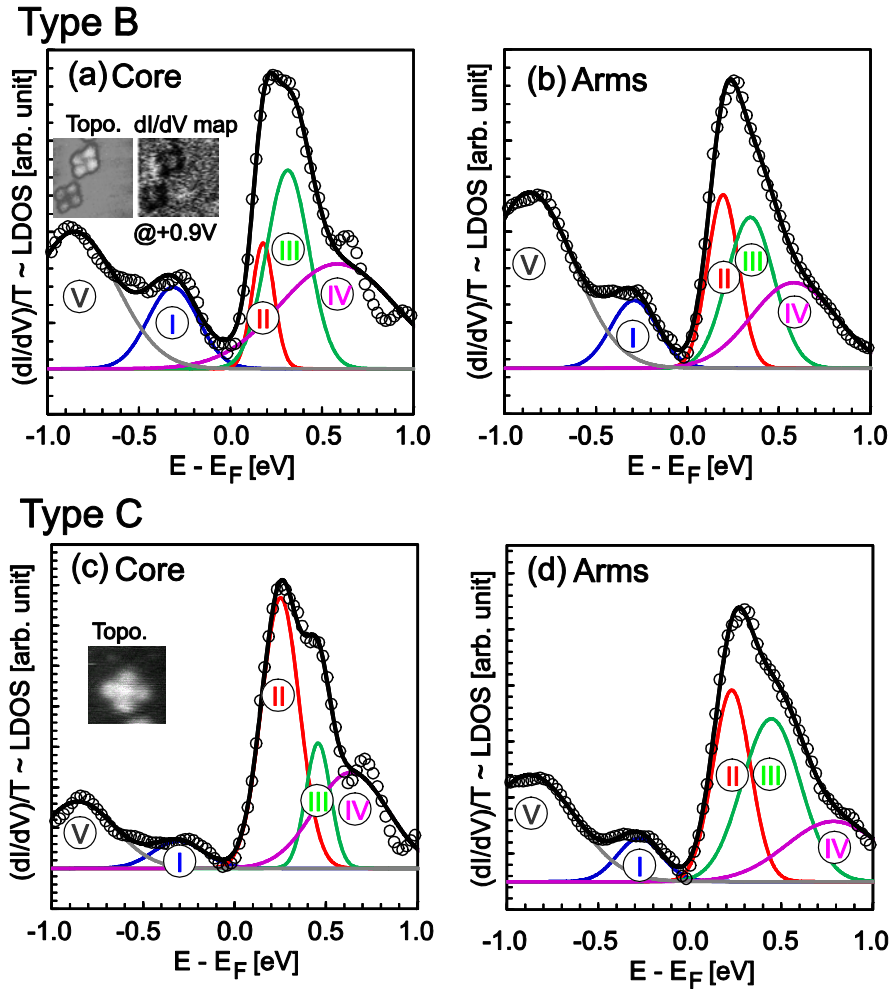


Fig.4: (color online)  $(dI/dV)/T$  curve (black circles) measurements at 300 K performed on the type B and C single  $\text{H}_2\text{Pc}$  molecules adsorbed on the Fe(001)-whisker. The  $(dI/dV)/T$  curves were fitted with Gaussian curves. The fitted curves are shown as black lines. Obtained Gaussian peaks were used to determine LDOS peak energy positions labeled I (blue), II (red), III (green), IV (pink), and V (grey). (a) and (b) were obtained for the type B molecule at the core and the arms inside the single molecule, respectively. Insets in (a) ( $5 \times 5$  nm) show a topographic image and a  $dI/dV$  map at +0.9 V. (c) and (d) were obtained for type C molecule at the core and the arms inside the single molecule, respectively. An inset in (c) ( $5 \times 5$  nm) shows a topographic image.

**Table 1**

Type	Area	Temp. [K]	Tip	Peak I [eV]	Peak II [eV]	Peak III [eV]	Peak IV [eV]	Peak V [eV]
A	core	7	No.1	-0.22±0.16	+0.10±0.05	+0.21±0.11	+0.53±0.23	none
A	core	300	No.2	-0.29±0.18	+0.14±0.08	+0.29±0.12	+0.52±0.18	-0.84±0.26
A	arms	300	No.2	-0.30±0.15	+0.18±0.09	+0.32±0.13	+0.56±0.25	-0.86±0.25
B	core	300	No.2	-0.31±0.16	+0.18±0.07	+0.31±0.14	+0.58±0.37	-0.85±0.28
B	arms	300	No.2	-0.29±0.15	+0.19±0.10	+0.34±0.15	+0.58±0.27	-0.86±0.28
C	core	300	No.2	-0.31±0.16	+0.25±0.12	+0.45±0.08	+0.64±0.24	-0.86±0.24
C	arms	300	No.2	-0.28±0.14	+0.23±0.12	+0.45±0.19	+0.79±0.30	-0.88±0.30

Table 1: Peak energy positions obtained by Gaussian fittings to the  $(dI/dV)/T$  curves experimentally obtained on the core and the arms of the type A, B, and C single H<sub>2</sub>Pc molecules on Fe(001). Error bars denote a half width of half maximum of each Gaussian peak.

Figure 5

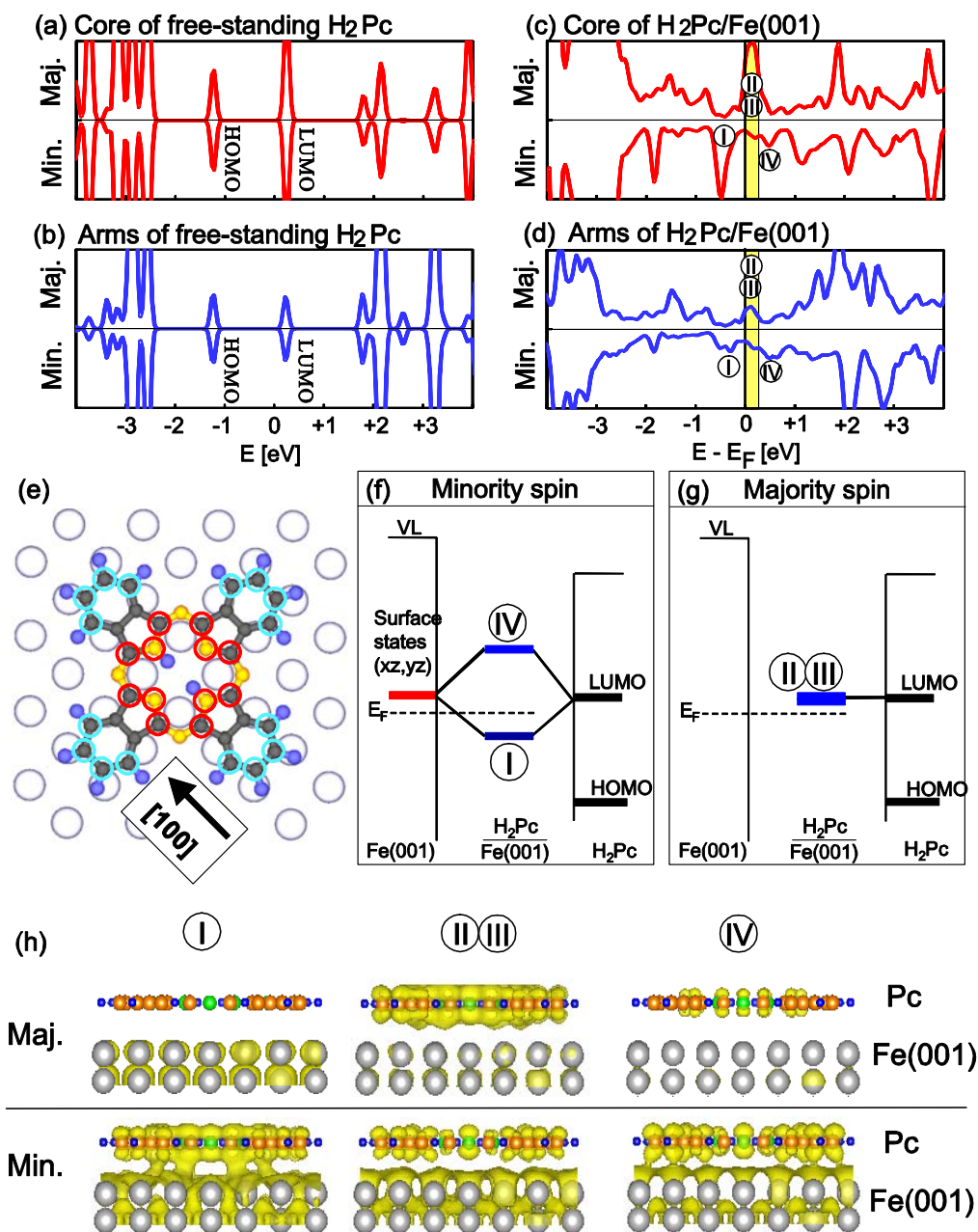


Fig.5: (color online) Calculated spin-resolved LDOS of (a,b) a free-standing  $H_2Pc$  molecule and (c,d) a single  $H_2Pc$  molecule (type A) adsorbed onto bcc  $Fe(001)$  substrate. The top and bottom sections show the majority and minority spin states, respectively. I, II, III and IV denote the energy positions of experimentally determined peaks. (e) Spherical model of a  $H_2Pc$  molecule on a square atomic lattice. H (blue sphere), C (grey sphere), and N (yellow sphere) form the constituent chemical species of the molecule. Four nitrogen and eight carbon atoms marked by the red circles are main contributed atoms for the core. 16 carbon atoms marked by the blue circles are representatives of the arms. (f,g) Interface hybridization between  $H_2Pc$  and  $Fe(001)$  in the minority (f) and the majority (g) spin states. In (f), energy positions of the  $Fe(001)$   $d_{xz+yz}$  surface states and the molecular HOMO/LUMO states are shown as red and black lines, respectively. Blue lines denote new hybridized bonding/antibonding states. I and IV denote experimentally obtained peak positions. In (g), no peak at the  $Fe(001)$  side. No hybridization occurs. (h) Three-dimensional views of minority and majority spin interface states: hybridized molecular  $\pi$  and  $Fe(001)$   $d$  states.

Figure 6

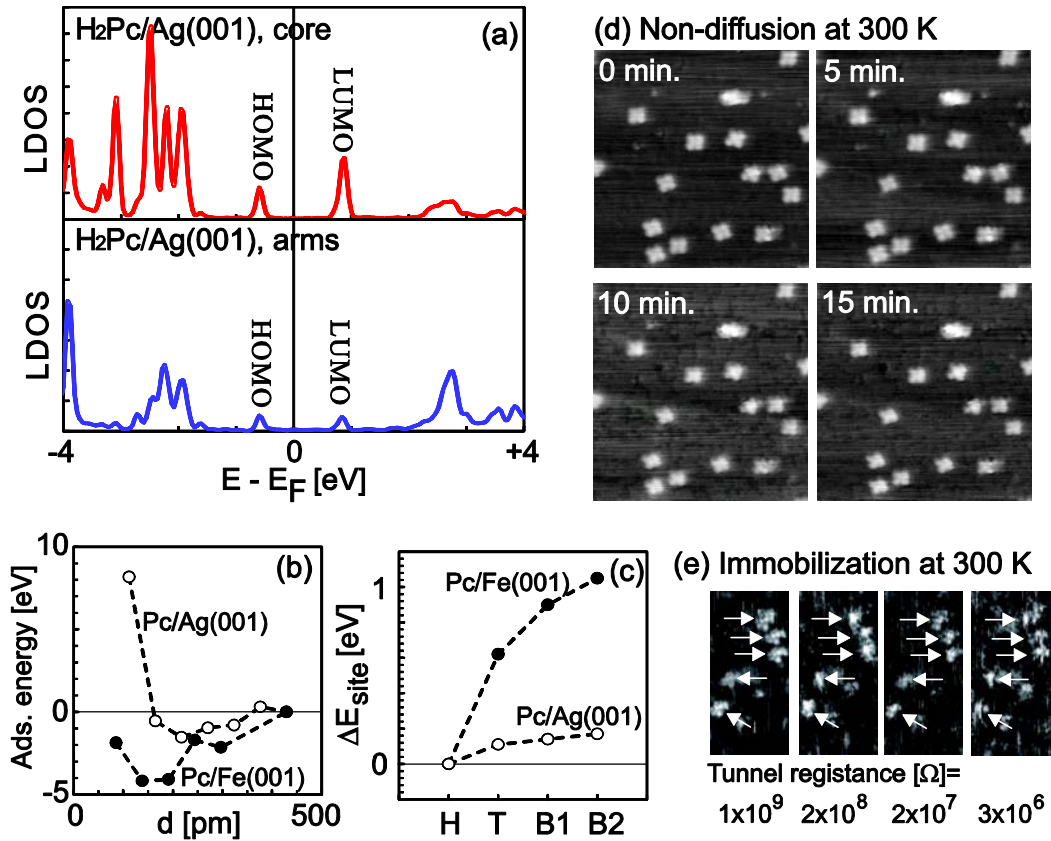


Fig.6: (a) Calculated LDOS of a single H<sub>2</sub>Pc molecule adsorbed onto a fcc Ag(001) substrate. (b) Adsorption energy of single H<sub>2</sub>Pc molecule onto Fe(001) (black dots) and Ag(001) (white dots). The  $d$  axis represents the molecule-substrate distance. (c) Energy difference of the diffusion barrier from the four-fold hollow site position (H) for H<sub>2</sub>Pc molecules on Ag(001) (white dots) and Fe(001) (black dots). A top site (T), a bridge site along the [010] direction (B1), and a bridge site along the [100] direction (B2) are calculated. (d) Continuous STM images of a given area on which 0.1 ML H<sub>2</sub>Pc was adsorbed onto Fe(001) observed at 300 K ( $V_s = -600$  mV,  $I = 600$  pA,  $20 \times 20$  nm). The images were sequentially acquired at 5-min intervals. (e) STM images ( $20 \times 9.4$  nm) of this area at different tunneling resistances of  $1 \times 10^9$  Ohms ( $V_s = -600$  mV,  $I = 600$  pA),  $2 \times 10^8$  Ohms ( $V_s = -600$  mV,  $I = 3$  nA),  $2 \times 10^7$  Ohms ( $V_s = -600$  mV,  $I = 30$  nA), and  $3 \times 10^6$  Ohms ( $V_s = -100$  mV,  $I = 30$  nA). Five single molecules (bright spots) did not move.